Memory Formation in Adaptive Networks

Komal Bhattacharyya,[1] David Zwicker,[1] and Karen Alim[2,1,*,†]
[1]Max Planck Institute for Dynamics and Self-Organisation, Göttingen 37077, Germany
[2]Center for Protein Assemblies (CPA), Physik-Department, Technische Universität München, Garching 85748, Germany

(Received 27 April 2021; revised 14 June 2022; accepted 15 June 2022; published 6 July 2022)

The continuous adaptation of networks like our vasculature ensures optimal network performance when challenged with changing loads. Here, we show that adaptation dynamics allow a network to memorize the position of an applied load within its network morphology. We identify that the irreversible dynamics of vanishing network links encode memory. Our analytical theory successfully predicts the role of all system parameters during memory formation, including parameter values which prevent memory formation. We thus provide analytical insight on the theory of memory formation in disordered systems.

DOI: 10.1103/PhysRevLett.129.028101

Network architecture determines network performance. Strengthening and weakening links in a network over time is key for maintaining optimal performance under changing loads for stability in mechanical networks [1–3] as well as transport efficiency in traffic [4,5] or vasculature [6–15]. Understanding the physical principles of how an adaptive network's past is governing its current state is eminent in a world where even social and economic networks are currently facing massive adaptation. For the prototype of adaptive networks, living flow networks, data evidences that changes in loads drive the permanent adaptation of network architecture [16–20]. Do adaptive networks memorize information about past loads while continuously striving for their optimal state?

Memory in disordered, passive systems, like granular media [21–23] or non-Brownian suspensions [24–26] as well as in neural networks [27,28], is encoded in persistent configurations of the microstructure of the system [29]. During a training period, irreversible dynamics lead to specific microstates; the system memorizes the past direction or amplitude of the training load. Do the active dynamics of the continuous optimization of adaptive networks allow for irreversibility to encode information about the past?

Adaptive flow networks [9,30–33], as well as adaptive mechanical [34–43] and resistor networks [44–47], can evolve individual link conductance to minimize a desired loss function like power loss [15,30,39,46–50]. This optimization is constrained by a fixed building cost. Particularly, the architecture and adaptation of living flow networks, like plant and animal vasculature, have been successfully described as optimal adaptive networks [15,30,46,47]. For animal vasculature, the adaptation dynamics of individual links [6,30] has even been substantiated experimentally [8,10]. These living adaptive networks are facing omnipresent fluctuations in loads [9,15,47,51–54], which might erase any memories encoded in the microstructure of a network.

Here, we show that adaptive networks retain information on the position of an applied load in their architecture. Despite the presence of fluctuating loads, the applied load's position is retrieved upon reapplication. Specifically, we find that links with vanishing conductivity are responsible for the irreversibility of optimization dynamics allowing for memory encoding. We analytically show that irreversibility is a direct consequence of the adaptation dynamics, providing deep insight into the physical role of all systems' parameters on memory. Strikingly, our analytical calculations predict that the cost function can limit memory formation, which we confirm in our simulation. Our Letter thus not only discovers that adaptive networks are able to store memories of previous loads but provides an analytical tractable theory of memory formation in disordered systems.

We follow the standard model for adaptive networks most often used in the context of flow networks [15,30,46–48,55,56]. The network consist of N nodes that are connected by links, whose flow rates Q_{ij} are linearly dependent on their conductances C_{ij} for fixed potential differences. At every time step t, the flow in the network is driven by loads $q_i(t)$ applied at each node i, where only one node has a negative load, $q_1(t) = -\sum_{i>1} q_i(t)$, i.e., it acts as the outlet, while all other nodes have $q_i(t) \geq 0$ [15,47]. Conservation of flow at every node, known as Kirchhoff's law, uniquely determines individual flow rates $Q_{ij}(t)$ from the entire network's conductances $C_{ij}(t)$ and the loads $q_i(t)$ at every node.

The adaptation rule first introduced by Murray [6] minimizes power loss $E = \sum_{\langle ij \rangle} Q_{ij}(t)^2 C_{ij}(t)^{-1}$ under the constraint of fixed building cost $\sum_{\langle ij \rangle} C_{ij}(t)^\gamma = \mathcal{K}^\gamma$. Here, $\mathcal{K}$ quantifies the overall constraint, and the exponent γ determines how link conductances contribute to the cost; see the Supplemental Material [57]. For example, resistor networks or porous media typically exhibit $\gamma = 1$, while flow networks with Hagen-Poiseuille flow have $\gamma = \frac{1}{2}$ or $\gamma = \frac{1}{4}$ when the overall tube volume or the surface area is fixed, respectively. Iterative adaptation of C_{ij} with discrete time steps δt locally solves the optimization problem [46,57]. To account for fluctuating loads $q_i(t)$, we additionally average over a period T, implying the update rule [15,47]

$$C_{ij}(t + \delta t) = \mathcal{K} A(t)^{-\frac{1}{\gamma}} \langle Q_{ij}(t)^2 \rangle_T^{\frac{1}{\gamma+1}}, \tag{1}$$

where $A(t) = \sum_{\langle ij \rangle} \langle Q_{ij}(t)^2 \rangle_T^{\gamma/(\gamma+1)}$ is a normalization factor. Taken together, this model defines how the conductances adapt for a given time series of loads $q_i(t)$ [57].

Memory is the storage of information in a noisy environment [29], so that previously written information can be retrieved at a later time. To probe for memory in adaptive networks, we consider a disk-shaped geometry with its primary outlet $i = 1$ at the center; see Fig. 1(a). We model the fluctuating environment by stochastically switching on and off background loads with equal probability, which describes open-close switches ubiquitous in biological flow networks [9,47]. The mean and the standard deviation of the fluctuations are parametrized by the average background load $q^{(0)}$ on every node. Note that our results are robust and also hold when we consider a different noise distribution or a continuous optimization algorithm; see the Supplemental Material [57].

To test for memory formation, we follow the protocol used in disordered systems [58,59], where a writing stimulus is applied and the information about the stimulus is subsequently retrieved by applying the full possible range of stimuli. In our case, we apply an additional load q^{add} at the boundary of the network at a particular angle θ_1 over a duration t_{train}. This stimulus imprints a treelike structure on the network morphology; see Fig. 1(a). However, the system quickly returns to a seemingly isotropic morphology when the additional load is removed; see Fig. 1(b). To test whether this morphology still carries information about the writing stimulus, we applied after a time period t_{wait} a probing stimulus at various angles θ_2 and measured the total power loss E. Figure 1(c) shows that the power loss is minimal for precisely the angle at which the writing stimulus was applied, indicating that this configuration is more optimized due to memory of the stimulus. In contrast, the power loss is independent of the angle in an untrained network where the writing stimulus was never applied. This demonstrates that adaptive networks can retain memory despite lacking an obvious visual imprint.

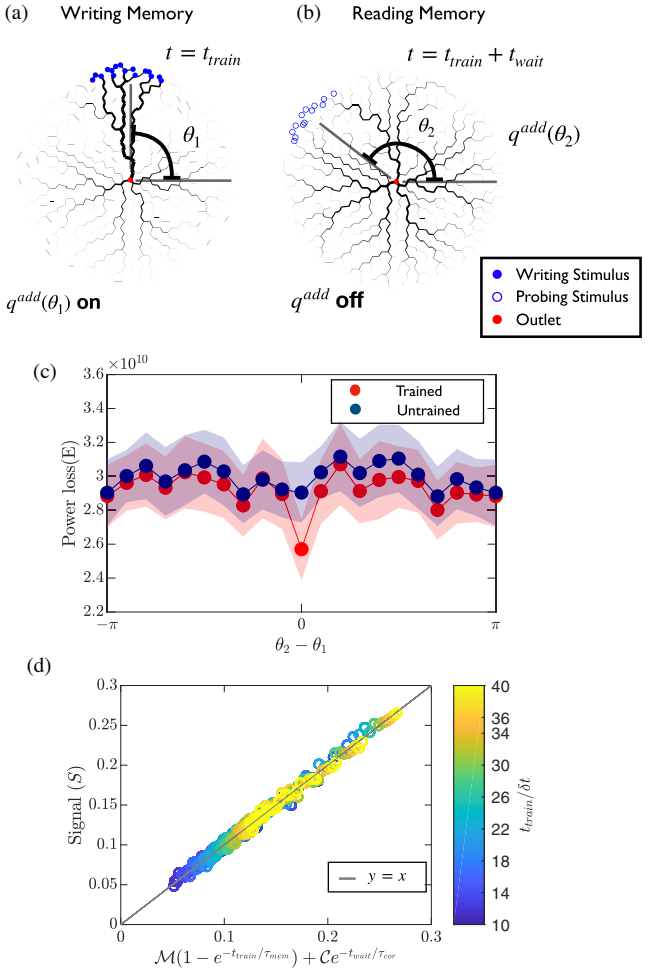

FIG. 1. Networks with $\gamma = \frac{1}{2}$ undergo memory formation and retrieval. (a) Network evolved under writing stimulus which is additional load q^{add}, equally distributed over outer nodes around θ_1 (blue filled), for training time t_{train}. Outlet node depicted in red. (b) Network adapted without stimulus over waiting time t_{wait}. Memory is subsequently probed by applying probing stimulus at angle θ_2 (empty blue). (c) Power loss E over 200 independent simulations versus $\theta_2 - \theta_1$ for varying θ_2 for trained dataset (red) and for untrained data set (blue). (d) Memory read-out signal S collapses when plotted using Eq. (3) for all t_{train} shown by the colorbar. ($\tau_{\text{mem}} = 29\delta t$, $\tau_{\text{cor}} = 7.5\delta t$). $q^{(0)} = 1$, $q^{\text{add}} = 2000 q^{(0)}$, $N = 1945$, and $T = 30\delta t$.

To unveil the mechanism of this memory, we quantify the memory read-out signal S as the relative change in power loss,

$$S = 1 - \frac{\langle E_{\text{trained}}(\theta_2 = \theta_1) \rangle}{\langle E_{\text{untrained}}(\theta_2 = \theta_1) \rangle}. \tag{2}$$

Strikingly, we find that data for different t_{train} and t_{wait} collapse onto a straight line of the form

$$S \approx \mathcal{M}(1 - e^{-t_{\text{train}}/\tau_{\text{mem}}}) + \mathcal{C} e^{-t_{\text{wait}}/\tau_{\text{cor}}}; \tag{3}$$

see Fig. 1(d). This functional form was motivated by an individual analysis of the dependencies [57]. The structure of the two terms suggests that the signal consists of persistent memory, $\mathcal{M}(1-e^{-t_{\rm train}/\tau_{\rm mem}})$, as well as correlations that decay over time, $\mathcal{C}e^{-t_{\rm wait}/\tau_{\rm cor}}$. Note that the correlations start at the maximal value $\mathcal{C}$ and decay with a time scale $\tau_{\rm cor}$ during the waiting period; see the Supplemental Material [57]. Conversely, memory builds up during the training period with a timescale $\tau_{\rm mem}$, saturates at the value $\mathcal{M}$, and is retained indefinitely.

To understand how adaptive networks can encode memory, we next quantify how the links' conductances C_{ij} evolve in time. Figure 2(a) shows that after the initial training period low conductance links tend to shrink, while high conductance links tend to stay the same. In fact, we observe that the weakest links eventually reach the minimal conductance value allowed in the simulation [see Figs. 2(b) and 2(c); details in the Supplemental Material [57]] and can never grow back under the adaptation dynamics given by Eq. (1), despite the background load fluctuations. We show in the Appendix that azimuthally oriented links decay fastest in the vicinity of the stimulus. Consequently, the orientations of irreversibly shrinking links retain memory of the spatial stimulus, comparable to memory formation in disordered systems [29].

Figure 2(a) suggests a simple functional form for the dynamics of the network: conductances C above a threshold value $C_{\rm th}$ fluctuate minimally to maintain fixed building costs [57], while those below shrink with a power law behavior:

$$\frac{C(t+\delta t)}{C(t)} \approx \begin{cases} \left[\frac{C(t)}{C_{\rm th}}\right]^{\beta} & C(t) < C_{\rm th} \\ 1 & C(t) \geq C_{\rm th}. \end{cases} \tag{4}$$

Fitting the data shown in Fig. 2(a), we find $\langle C(t+\delta t)/C(t)\rangle = 1 \pm 0.03$ for large conductances and $\beta = 0.31 \pm 0.07$ for small conductances in the case without stimulus (colored dots). Remarkably, we find a very similar exponent ($\beta = 0.31 \pm 0.07$) when a stimulus is present (gray dots), although the threshold value $C_{\rm th}$ is clearly lower. This suggests that the exponent β is constant and characterizes the adaptation dynamics of the network, while $C_{\rm th}$ depends on the stimulus strength. These observations point to the dynamics of small conductance links as key for memory formation in adaptive networks. The irreversible dynamics break ergodicity [57], implying that not all configurations can be explored in the long time limit and memory persists.

To show that the links' dynamics observed in the numerical simulations are universal, we next consider the dynamics of the simplest adaptive networks analytically. For simplicity, we focus here on constraints with $\gamma = \frac{1}{2}$, but the general case is discussed in the Supplemental Material [57]. We start by considering the simplest network consisting of three nodes in a triangular arrangement; see Fig. 3(a). For given loads q_2 and q_3, the optimal network has a V-shaped morphology [46] with a negligible conductance between nodes 2 and 3. We then perturb the system around the optimal state by altering the load at node 2 to $q_2 + \delta q$ and examine the adaptation of all conductances under the dynamics given by Eq. (1). We derive that the high conductance links barely change [57],

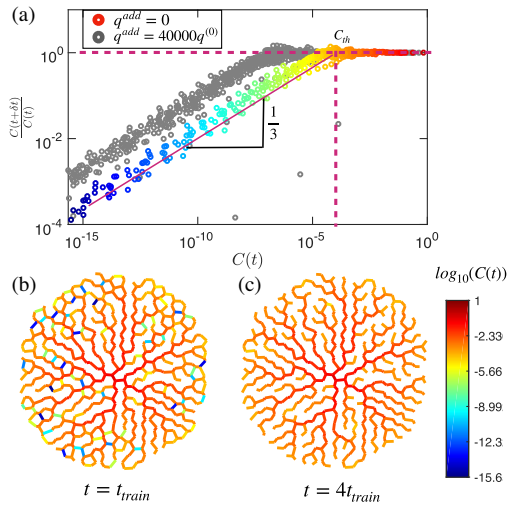

FIG. 2. (a) Ratio of conductance of two subsequent iterations versus preceding conductance during adaptation for $3t_{\rm train}$ iterations after training phase of duration $t_{\rm train}$ ended. Above threshold conductance $C_{\rm th}$ (vertical red dashed line) conductances fluctuate around $[C(t+\delta t)/C(t)] = 1$ (horizontal red dashed line). Low conductance links follow a power law with exponent $1/3$ (red line). Only threshold conductance $C_{\rm th}$ is stimulus strength specific; compare gray ($q^{\rm add} = 40000q^{(0)}$) and color ($q^{\rm add} = 0$). (b) A network adapted for $t_{\rm train}$, iterating for longer, $4t_{\rm train}$, links with conductance smaller than threshold $C_{\rm th}$ disappear (c). $\gamma = 1/2$, $q^{(0)} = 1$, $N = 526$, and $T = 30\delta t$.

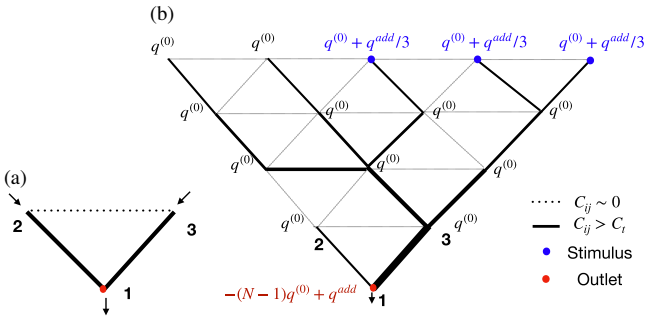

FIG. 3. Optimized networks for analytical calculations. (a) Simplest network, with one link (dotted line) of vanishingly small conductance. Nodes 2 and 3 bear positive load balanced by outlet node 1 (red dot). (b) General asymmetric network, where all nodes of the upper layers are connected to node 3. $q^{(0)}$ mean fluctuating load on all the nodes, blue dots denote stimulus of additional load $q^{\rm add}$ distributed among those nodes.

$$\frac{C_{12}(t+\delta t)}{C_{12}(t)} = \frac{C_{13}(t+\delta t)}{C_{13}(t)} = 1 + \mathcal{O}\left(\frac{\delta q}{q_2}\right). \tag{5}$$

Conversely, the small conductance changes as

$$\frac{C_{23}(t+\delta t)}{C_{23}(t)} = \left[\frac{C_{23}(t)}{C_{\mathrm{th}}}\right]^{\frac{1}{3}}, \tag{6}$$

where the threshold C_{th} is proportional to the constraint $\mathcal{K}$ and otherwise only depends on the loads [57]. This analytical result qualitatively agrees with the numerical results presented in Fig. 2(a). In particular, we predict an exponent of $\frac{1}{3}$ for the evolution of small conductances.

To show that the analytical result is universal and to study the parameter dependence of the threshold value C_{th}, we next extend the analytical treatment to larger networks; see the Supplemental Material [57]. Here, we build more complex trees by adding additional layers. Since the dynamics of C_{23} are governed by the load difference between node 2 and node 3, we first focus on fully asymmetric trees, where the load difference is maximized by funneling all additional loads through node 3; see Fig. 3(b). For simplicity, we consider a scenario described by an additional load q^{add} applied at the last layer, while the fluctuations are represented by their average value $q^{(0)}$ at each node and load perturbation at node 2 of δq. This implies $q_2(t) = q^{(0)} + \delta q$ and $q_3(t) = (N-2)q^{(0)} + q^{\mathrm{add}}$. Focusing on the adaptation dynamics of the small conductance C_{23}, we again find the power law with exponent $\frac{1}{3}$, and the associated threshold value reads as

$$C_{\mathrm{th}} \approx \frac{\mathcal{K}}{(1+\frac{\delta q}{q^{(0)}})^4 (N + \frac{q^{\mathrm{add}}}{q^{(0)}})^{\frac{4}{3}}}, \tag{7}$$

assuming $q_2 \ll q_3$; see the Supplemental Material [57]. This expression demonstrates how the additional load q^{add} and load perturbation δq compete with the average of the background load fluctuations quantified by $q^{(0)}$: Larger perturbations, a stronger stimulus, and a larger system size N result in a smaller threshold, slowing down the decay of weak links. Conversely, a larger average background load increases the threshold, allowing for a fast decay of weak links. We find very similar results for fully symmetric trees, suggesting that all treelike networks exhibit this behavior; see the Supplemental Material [57].

Despite the simplicity of the considered networks, our analytical results agree with the numerical data shown in Fig. 2(a). In particular, they confirm that high conductance links are invariant, while links with a conductance below the threshold C_{th} shrink with a $\frac{1}{3}$-power law. Moreover, Eq. (7) predicts how the model parameters affect the dynamics of links leading to memory formation in adaptive networks. The analytical result suggests that links of weak conductance have universal ensemble dynamics governed only by the threshold C_{th} given by Eq. (7). To test this prediction, we quantified C_{th} by fitting the dynamics of the conductances as a function of N for various $q^{(0)}$ and q^{add}. Figure 4 confirms that the scaling predicted by Eq. (7) agrees with numerical simulations despite the simulation's more complex network morphology; see also the Supplemental Material [57]. We further confirm that C_{th} is independent of background load fluctuation in the absence of a stimulus q^{add} (see the Supplemental Material [57]), and the memory effect is independent of load fluctuation when $q^{\mathrm{add}}/q^{(0)}$ is kept constant [57], as predicted by Eq. (7).

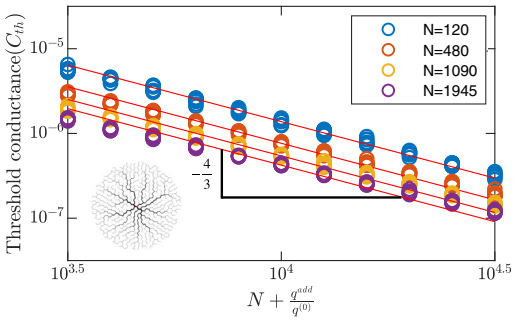

FIG. 4. Numerically determined threshold conductance C_{th} of disk-shaped networks (inset) follows analytical prediction on model parameters; compare Eq. (7). $\gamma = 1/2, T = 30\delta t$.

We have shown that adaptive networks, which minimize power loss under the constraint of constant building cost, exhibit memory. However, so far we have focused on the particular constraint parameter $\gamma = \frac{1}{2}$, which is known to result in treelike optimal morphologies [30,46,48,55], or hierarchical morphologies with loops [15,47,60] ignoring that other constraints are also possible and often lead to quite different optimal solutions [15,30,46,47,50,60]. How does memory formation change if we consider a general constraint parameter γ? Our detailed calculations (see the Supplemental Material [57]) reveal that the dynamics of high conductance links are independent of γ. Conversely, weak links follow the γ-dependent power law

$$\frac{C(t+\delta t)}{C(t)} \propto C(t)^{\frac{1-\gamma}{1+\gamma}}, \tag{8}$$

which reveals that weak links shrink faster for smaller γ. This equation indicates that memory exists for $\gamma < 1$ and the precise value of γ hardly affects the dynamics. Conversely, Eq. (8) predicts that weak links grow for $\gamma > 1$. Consequently, links never disappear, loops form [60], and memory formation should be impossible in this case. In fact, we expect that these systems are ergodic (see the Supplemental Material [57]), so that transient changes are erased in the long term.

To test memory formation in these systems, we performed numerical simulations with $\gamma = 1$. Figure 5 reveals that the

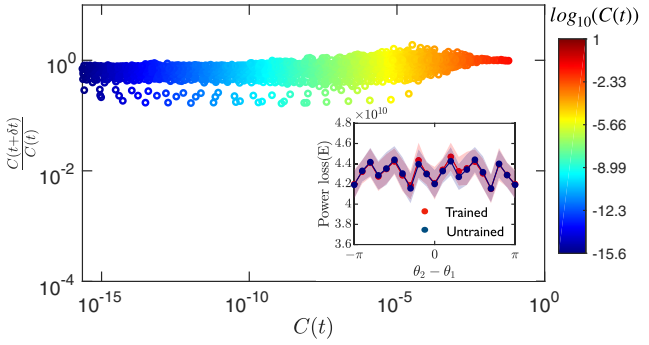

FIG. 5. Memory formation is absent when the cost function scales with $\gamma = 1$. In this case, all links are stable and the power loss E in trained and untrained network is identical (inset). Same protocol as in Fig. 1(c).

dynamics of the links hardly depend on their conductances C, implying that weak links typically do not vanish. These qualitatively different dynamics result in loopy networks, in contrast to the treelike networks that are observed for $\gamma = \frac{1}{2}$ [47]. Numerical simulations also show that the networks do not retain any memory of the direction of the stimulus; see the inset of Fig. 5 and the Supplemental Material [57]. Taken together, the analytical results and the numerical simulations indicate that memory formation relies on vanishing weak links and is only possible for $\gamma < 1$.

We have shown that adaptive networks can retain memory of a stimulus despite background load fluctuations. Applied loads lead to irreversible change in the networks' microstructure by eroding weak links that cannot be revived. Our analytical calculations and numerical simulations consistently describe a power law for the decay rate of low conductances, functionally determined by the networks' building cost. The irreversibility of the dynamics arises from the trade-off between building cost constraint and minimizing power loss. A high local load increases conductances locally for efficient flow while also eroding weak, unimportant links due to the constraint of a fixed building cost, thereby imprinting memory. Yet, if the cost to build high conductance links is too high ($\gamma \geq 1$) networks adapt to low hierarchy, loopy architecture, which erases memories of loads over time. Future work needs to show whether memory is also erased in adaptive networks on growing tissue, which achieve the global optimum [61], or in adaptive networks with the special ability to create new links [62].

Unraveling how adaptive networks can encode memories changes our physical understanding of these active systems. In particular, it provides a conceptional change in how we may look at and control adaptive networks when designing smart mechanical materials or treating the plethora of malfunctions of our very own vasculature.

This work was supported by the Max Planck Society. This project has received funding from the European Research Council (ERC) under the European Union's Horizon 2020 research and innovation program (Grant Agreement No. 947630, FlowMem).

Appendix: Spatial signature of memory.—To unveil the spatial signature of memory, we analyze the location of the shrinking weak links, which contain the memory, in detail. Our analytical calculations [57] indicate that links with a direct path from inlets to the outlet shrink more easily if they are far away from the stimulus. Conversely, links perpendicular to such direct paths decay quickly if they are close to the stimulus. We thus expect that azimuthally oriented links decay quickly close to the stimulus in our disk-shaped networks. To quantify this, we measure the fraction of minimal conductance links with radial positions between $R - \Delta r$ and R, where R is the radius of the network and Δr the width of the annulus. With stimulus, the network has a significantly higher fraction of such minimal links where the stimulus was applied; see Fig. 7(d). To get further details, we also measure the orientation of minimal link ij (see Fig. 6) as the angle $\phi_{ij} \in [0, (\pi/2)]$ between its orientation vector $\hat{X}^0_{ij}$ and its location vector $\vec{X}^l_{ij}$,

$$\phi_{ij} = \sin^{-1}\left(\frac{\|\vec{X}^l_{ij} \times \vec{X}^o_{ij}\|}{\|\vec{X}^l_{ij}\|\|\vec{X}^o_{ij}\|}\right). \tag{A1}$$

Consequently, $\phi_{ij} = 0$ corresponds to radially oriented links, while $\phi_{ij} = (\pi/2)$ indicates azimuthally oriented links.

We quantify the angle averaged over small regions of space in networks evolved without [Fig. 7(e)] and with a

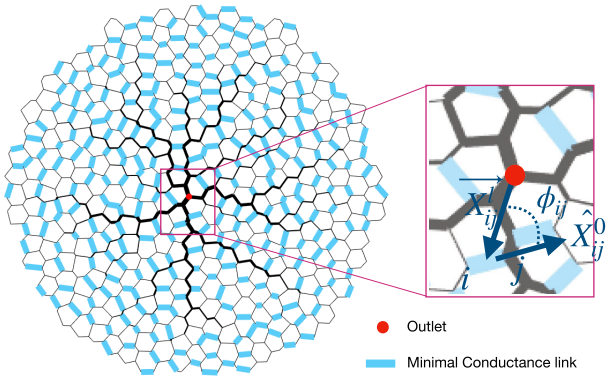

FIG. 6. Measure of vanishing link orientation for spatial signature of memory. Example network, highlighting vanishing links in light blue. Other links' width is scaled by their conductance value, and the outlet node is depicted in red. On network enlargement, a link orientation angle ϕ_{ij} (dark blue dotted curve) is indicated as the angle between the orientation vector $\vec{X}^0_{ij}$ of link ij and the location vector of the center of the considered link ij with respect to the outlet in the network ($\vec{X}^l_{ij}$).

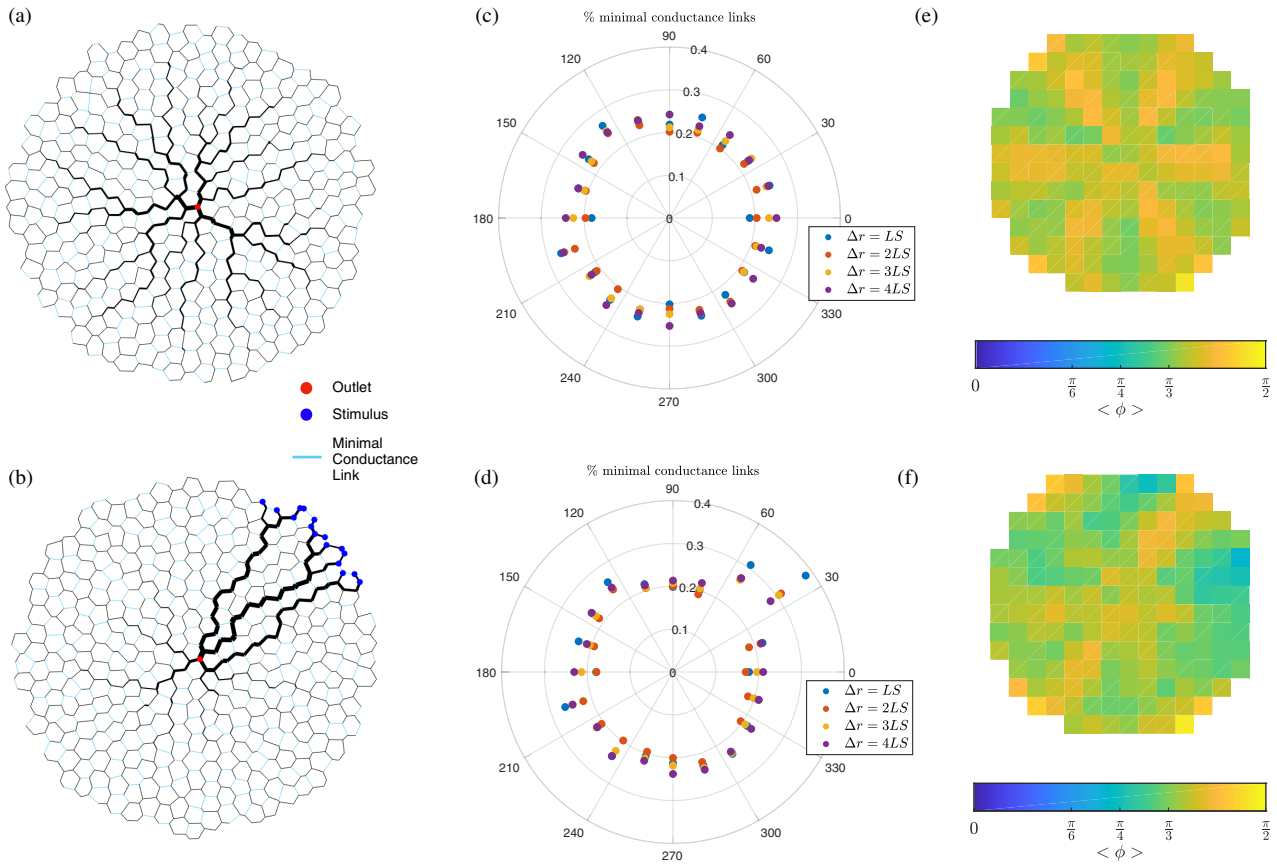

FIG. 7. Minimal conductance links retain spatial imprint of stimulus in the network morphology. (a) Example network evolved without any stimulus. Light blue links in the network represent links with minimal conductance. (b) Example network evolved with a stimulus equally distributed over the blue filled nodes. (c),(d) Average fraction of weak links at rim of width Δr of the network as a function of polar angle (c) for networks without stimuli and (d) for networks evolved with stimulus applied in (b). Data for various Δr, measured in terms of the average distance, LS, between neighboring nodes, is shown as an average of 100 runs. (e), (f) Average angle between orientation vector and location vector (with respect to the center of the network) of minimal conductance links evaluated over a discrete grid (e) for networks without any stimulus and (f) for networks evolved with stimulus applied in (b). Averages are over 80 independent runs. Additional model parameters: $q^{\mathrm{add}} = 2000q^{(0)}$, $q^{(0)} = 1$, $N = 1945$, $t = 25\delta t$, and $\gamma = 0.5$.

stimulus [Fig. 7(f)]. While both plots reveal the sixfold symmetry of the underlying irregular network, there are also significant differences: The average orientation $\langle\phi\rangle$ is slightly higher in the wedge defined by the stimulus, indicating that azimuthally oriented links are more likely to decay. Conversely, $\langle\phi\rangle$ is slightly reduced at the boundary of this region, in agreement with our analytical calculations [57]. Taken together, our analysis shows that the decay of azimuthally oriented links in the vicinity of the stimulus memorizes its location.

*To whom all correspondence should be addressed.
†k.alim@tum.de

[1] H. N. Motlagh, J. O. Wrabl, J. Li, and V. J. Hilser, The ensemble nature of allostery, Nature (London) **508**, 331 (2014).
[2] A. A. S. T. Ribeiro and V. Ortiz, A chemical perspective on allostery, Chem. Rev. **116**, 6488 (2016).
[3] M. D. Daily and J. J. Gray, Local motions in a benchmark of allosteric proteins, Proteins **67**, 385 (2007).
[4] A. Sims and K. Dobinson, The Sydney coordinated adaptive traffic (SCAT) system philosophy and benefits, IEEE Trans. Veh. Technol. **29**, 130 (1980).
[5] A. Pascale, H. T. Lam, and R. Nair, Characterization of network traffic processes under adaptive traffic control systems, Transp. Res. Proc. **9**, 205 (2015).
[6] C. D. Murray, The physiological principle of minimum work: II. Oxygen exchange in capillaries, Proc. Natl. Acad. Sci. U.S.A. **12**, 299 (1926).
[7] C. D. Murray, The physiological principle of minimum work, J. Gen. Physiol. **14**, 445 (1931).
[8] Q. Chen, L. Jiang, C. Li, D. Hu, J.-w. Bu, D. Cai, and J.-l. Du, Haemodynamics-driven developmental pruning of brain vasculature in zebrafish, PLoS Biol. **10**, e1001374 (2012).
[9] D. Hu, D. Cai, and A. V. Rangan, Blood vessel adaptation with fluctuations in capillary flow distribution, PLoS One **7**, e45444 (2012).

[10] W. W. Sugden, R. Meissner, T. Aegerter-Wilmsen, R. Tsaryk, E. V. Leonard, J. Bussmann, M. J. Hamm, W. Herzog, Y. Jin, L. Jakobsson, C. Denz, and A. F. Siekmann, Endoglin controls blood vessel diameter through endothelial cell shape changes in response to haemodynamic cues, Nat. Cell Biol. **19**, 653 (2017).
[11] K. A. McCulloh, J. S. Sperry, and F. R. Adler, Water transport in plants obeys Murray's law, Nature (London) **421**, 939 (2003).
[12] K. Alim, Fluid flows shaping organism morphology, Phil. Trans. R. Soc. B **373**, 20170112 (2018).
[13] T. Nakagaki, H. Yamada, and Á. Tóth, Maze-solving by an amoeboid organism, Nature (London) **407**, 470 (2000).
[14] T. Nakagaki, Smart behavior of true slime mold in a labyrinth, Res. Microbiol. **152**, 767 (2001).
[15] E. Katifori, G. J. Szöllősi, and M. O. Magnasco, Damage and Fluctuations Induce Loops in Optimal Transport Networks, Phys. Rev. Lett. **104**, 048704 (2010).
[16] A. Ames, R. L. Wright, M. Kowada, J. M. Thurston, and G. Majno, Cerebral ischemia. II. The no-reflow phenomenon, Am. J. Pathol. **52**, 437 (1968), https://www.ncbi.nlm.nih.gov/pmc/articles/PMC2013326/.
[17] P. Khatri, J. Neff, J. P. Broderick, J. C. Khoury, J. Carrozzella, and T. Tomsick, Revascularization end points in stroke interventional trials, Stroke **36**, 2400 (2005).
[18] M. Nour, F. Scalzo, and D. S. Liebeskind, Ischemia-reperfusion injury in stroke, Interv. Neurol. **1**, 185 (2012).
[19] S. Wegener, Improving cerebral blood flow after arterial recanalization: A novel therapeutic strategy in stroke, Int. J. Mol. Sci. **18**, 2669 (2017).
[20] M. Kramar and K. Alim, Encoding memory in tube diameter hierarchy of living flow network, Proc. Natl. Acad. Sci. U.S.A. **118**, e2007815118 (2021).
[21] M. Toiya, J. Stambaugh, and W. Losert, Transient and Oscillatory Granular Shear Flow, Phys. Rev. Lett. **93**, 088001 (2004).
[22] N. W. Mueggenburg, Behavior of granular materials under cyclic shear, Phys. Rev. E **71**, 031301 (2005).
[23] J. Ren, J. A. Dijksman, and R. P. Behringer, Reynolds Pressure and Relaxation in a Sheared Granular System, Phys. Rev. Lett. **110**, 018302 (2013).
[24] F. Gadala-Maria and A. Acrivos, Shear-induced structure in a concentrated suspension of solid spheres, J. Rheol. **24**, 799 (1980).
[25] M. D. Haw, W. C. K. Poon, P. N. Pusey, P. Hebraud, and F. Lequeux, Colloidal glasses under shear strain, Phys. Rev. E **58**, 4673 (1998).
[26] G. Petekidis, A. Moussaïd, and P. N. Pusey, Rearrangements in hard-sphere glasses under oscillatory shear strain, Phys. Rev. E **66**, 051402 (2002).
[27] J. J. Hopfield, Neural networks and physical systems with emergent collective computational abilities., Proc. Natl. Acad. Sci. U.S.A. **79**, 2554 (1982).
[28] J. J. Hopfield and D. W. Tank, "Neural" computation of decisions in optimization problems, Biol. Cybern. **52**, 141 (1985).
[29] N. C. Keim, J. D. Paulsen, Z. Zeravcic, S. Sastry, and S. R. Nagel, Memory formation in matter, Rev. Mod. Phys. **91**, 035002 (2019).
[30] D. Hu and D. Cai, Adaptation and Optimization of Biological Transport Networks, Phys. Rev. Lett. **111**, 138701 (2013).
[31] A. Tero, R. Kobayashi, and T. Nakagaki, Physarum solver: A biologically inspired method of road-network navigation, Physica A (Amsterdam) **363A**, 115 (2006).
[32] J. Gräwer, C. D. Modes, M. O. Magnasco, and E. Katifori, Structural self-assembly and avalanchelike dynamics in locally adaptive networks, Phys. Rev. E **92**, 012801 (2015).
[33] H. Ronellenfitsch and E. Katifori, Phenotypes of Vascular Flow Networks, Phys. Rev. Lett. **123**, 248101 (2019).
[34] C. P. Goodrich, A. J. Liu, and S. R. Nagel, The Principle of Independent Bond-Level Response: Tuning by Pruning to Exploit Disorder for Global Behavior, Phys. Rev. Lett. **114**, 225501 (2015).
[35] M. M. Driscoll, B. G.-g. Chen, T. H. Beuman, S. Ulrich, S. R. Nagel, and V. Vitelli, The role of rigidity in controlling material failure, Proc. Natl. Acad. Sci. U.S.A. **113**, 10813 (2016).
[36] H. Flechsig, Design of elastic networks with evolutionary optimized long-range communication as mechanical models of allosteric proteins, Biophys. J. **113**, 558 (2017).
[37] J. W. Rocks, N. Pashine, I. Bischofberger, C. P. Goodrich, A. J. Liu, and S. R. Nagel, Designing allostery-inspired response in mechanical networks, Proc. Natl. Acad. Sci. U.S.A. **114**, 2520 (2017).
[38] L. Yan, R. Ravasio, C. Brito, and M. Wyart, Architecture and coevolution of allosteric materials, Proc. Natl. Acad. Sci. U.S.A. **114**, 2526 (2017).
[39] J. W. Rocks, H. Ronellenfitsch, A. J. Liu, S. R. Nagel, and E. Katifori, Limits of multifunctionality in tunable networks, Proc. Natl. Acad. Sci. U.S.A. **116**, 2506 (2019).
[40] W. G. Ellenbroek, Z. Zeravcic, W. Van Saarloos, and M. Van Hecke, Non-affine response: Jammed packings vs. spring networks, Europhys. Lett. **87**, 34004 (2009).
[41] D. R. Reid, N. Pashine, J. M. Wozniak, H. M. Jaeger, A. J. Liu, S. R. Nagel, and J. J. de Pablo, Auxetic metamaterials from disordered networks, Proc. Natl. Acad. Sci. U.S.A. **115**, E1384 (2018).
[42] D. Hexner, A. J. Liu, and S. R. Nagel, Role of local response in manipulating the elastic properties of disordered solids by bond removal, Soft Matter **14**, 312 (2018).
[43] M. Stern, M. B. Pinson, and A. Murugan, Continual Learning of Multiple Memories in Mechanical Networks, Phys. Rev. X **10**, 031044 (2020).
[44] M. Durand, J.-F. Sadoc, and D. Weaire, Maximum electrical conductivity of a network of uniform wires: the Lemlich law as an upper bound, Proc. R. Soc. A **460**, 1269 (2004).
[45] M. Durand and D. Weaire, Optimizing transport in a homogeneous network, Phys. Rev. E **70**, 046125 (2004).
[46] S. Bohn and M. O. Magnasco, Structure, Scaling, and Phase Transition in the Optimal Transport Network, Phys. Rev. Lett. **98**, 088702 (2007).
[47] F. Corson, Fluctuations and Redundancy in Optimal Transport Networks, Phys. Rev. Lett. **104**, 048703 (2010).
[48] M. Durand, Structure of Optimal Transport Networks Subject to a Global Constraint, Phys. Rev. Lett. **98**, 088701 (2007).

[49] S.-S. Chang and M. Roper, Minimal transport networks with general boundary conditions, SIAM J. Appl. Math. **78**, 1511 (2018).

[50] J. B. Kirkegaard and K. Sneppen, Optimal Transport Flows for Distributed Production Networks, Phys. Rev. Lett. **124**, 208101 (2020).

[51] B. Klitzman, D. N. Damon, R. J. Gorczynski, and B. R. Duling, Augmented tissue oxygen supply during striated muscle contraction in the hamster. Relative contributions of capillary recruitment, functional dilation, and reduced tissue PO2, Circul. Res. **51**, 711 (1982).

[52] J. B. Delashaw and B. R. Duling, A study of the functional elements regulating capillary perfusion in striated muscle, Microvasc. Res. **36**, 162 (1988).

[53] T. E. Sweeney and I. H. Sarelius, Arteriolar control of capillary cell flow in striated muscle, Circul. Res. **64**, 112 (1989).

[54] D. Peak, J. D. West, S. M. Messinger, and K. A. Mott, Evidence for complex, collective dynamics and emergent, distributed computation in plants, Proc. Natl. Acad. Sci. U.S.A. **101**, 918 (2004).

[55] J. R. Banavar, F. Colaiori, A. Flammini, A. Maritan, and A. Rinaldo, Topology of the Fittest Transportation Network, Phys. Rev. Lett. **84**, 4745 (2000).

[56] M. Durand, Architecture of optimal transport networks, Phys. Rev. E **73**, 016116 (2006).

[57] See Supplemental Material at http://link.aps.org/supplemental/10.1103/PhysRevLett.129.028101 for clarification of adaptation rule, tests of memory formation on networks adapting with different load fluctuations and different adaptation rules. It contains clarifications about obtained fit parameters, for fitting memory signal with memory protocol parameters and details of analytical calculations of link dynamics.

[58] N. C. Keim and S. R. Nagel, Generic Transient Memory Formation in Disordered Systems with Noise, Phys. Rev. Lett. **107**, 010603 (2011).

[59] E. M. Schwen, M. Ramaswamy, C.-M. Cheng, L. Jan, and I. Cohen, Embedding orthogonal memories in a colloidal gel through oscillatory shear, Soft Matter **16**, 3746 (2020).

[60] F. Kaiser, H. Ronellenfitsch, and D. Witthaut, Discontinuous transition to loop formation in optimal supply networks, Nat. Commun. **11**, 5796 (2020).

[61] H. Ronellenfitsch and E. Katifori, Global Optimization, Local Adaptation, and the Role of Growth in Distribution Networks, Phys. Rev. Lett. **117**, 138301 (2016).

[62] T. W. Secomb, J. P. Alberding, R. Hsu, M. W. Dewhirst, and A. R. Pries, Angiogenesis: An adaptive dynamic biological patterning problem, PLoS Comput. Biol. **9**, e1002983 (2013).